Journal of Hazardous Materials 193 (2011) 128–138

Contents lists available at ScienceDirect

Journal of Hazardous Materials

journal homepage: www.elsevier.com/locate/jhazmat

Oxidative degradation kinetics and products of chlortetracycline by manganese dioxide

Gao Chen[a,b,1], Ling Zhao[a,b,*], Yuan-hua Dong[a,b]

[a] Key Laboratory of Soil Environment and Pollution Remediation, Institute of Soil Science, Chinese Academy of Sciences, Nanjing 210008, China
[b] Institute of Soil Science, Chinese Academy of Sciences-Hong Kong Baptist University (ISSAS-HKBU) Joint Laboratory on Soil and Environment, Nanjing 210008, China

ARTICLE INFO

Article history:
Received 11 January 2011
Received in revised form 28 June 2011
Accepted 10 July 2011
Available online 26 July 2011

Keywords:
Abiotic degradation
Chlortetracycline
δ-MnO_2
Kinetics
Products

ABSTRACT

This study investigated the abiotic transformation kinetics of chlortetracycline (CTC) by synthesized δ-MnO_2 under conditions of different solutions. CTC was rapidly oxidized by δ-MnO_2, with the generation of Mn^{2+}. The measured CTC transformation rate increased considerably with an increase in initial δ-MnO_2 concentration but it decreased as the initial CTC concentration increased. Both the measured CTC transformation rate and the amount of Mn^{2+} generated decreased with increasing pH. The CTC transformation rate rose with an increase in temperature. The apparent activation energy ($45 \pm 14\,kJ\,mol^{-1}$) was consistent with a surface-controlled reaction. Dissolved Mn^{2+} and Zn^{2+}, as background cations, and substituted phenols, as co-solutes, remarkably decreased the transformation rate of CTC. Liquid chromatography–tandem mass spectrometry (LC–MS-MS) was used to identify oxidation products, which include *iso*-CTC, 4-epi-CTC, anhydro-CTC and 4-epi-anhydro-CTC, keto-CTC, 4-epi-keto-CTC, *N*-demethyl-CTC, 4-epi-*N*-demethyl-CTC, *N*-didemethyl-CTC and 4-epi-*N*-didemethyl-CTC. Product identification together with Fourier transform-infrared (FTIR) spectra suggested that the hydroxyl groups at C6 and C12 and the dimethylamine group of CTC reacted with the Mn–OH groups on the δ-MnO_2 surface. Thus, δ-MnO_2 in the soils most probably plays an important role in the abiotic transformation of tetracycline antibiotics.

1. Introduction

Antibiotics are largely consumed by humans for therapeutic purposes and are widely used in livestock and poultry production, as well as in fish farming, for preventing illness or improving growth efficiency [1,2]. The increasing use of these drugs during the last five decades has caused genetic selection of more harmful bacteria—a matter of tremendous concern [3,4]. A representative of the group of tetracycline (TC) antibiotics, chlortetracycline (CTC) is globally used in the livestock industry because of its low cost and broad-spectrum range of antimicrobial activities. Up to 75% CTC of an administered CTC dose, however, can be excreted as the parent compound through animal urine and feces [5]. The most important ways by which antibiotics are introduced into the soil environment are through the use and dispersion of manure and sewage sludge in fields as fertilizers. CTC residues can be detected in manure, soil, water and sediment samples [6–8]. CTC was reported to be detected at levels between 100 and 7730 $\mu g\,kg^{-1}$ in manure samples examined by Hamscher et al. [9]. The concentration level of CTC was up to 150 $\mu g\,kg^{-1}$ in soil amended with contaminated manure [10]. Such considerable amounts of CTC residues in manure and soil would result in the emergence and spread of resistant microorganisms and they could also be absorbed by certain crops such as corn, green onion and cabbage [11], which could have potential impacts on the ecosystems and the human health [12].

TC antibiotics can persist in terrestrial and aquatic environments because of their intensive usage and high adsorption capability [13]. Under field conditions, Halling-Sørensen et al. [14] found that the average degradation half-lives of CTC varied from 25 to 34 days in two Danish sandy soils. Samuelsen et al. [15] reported that no degradation was observed after 6 months' incubation in a laboratory study of oxytetracycline (OTC) in marine sediment. The biodegradation rates of most antibiotics were relatively lower than their abiotic degradation rates because they are specially designed and produced to inhibit or destroy microbial growth [16]. Abiotic degradation of antibiotics, such as photodegradation and oxidative degradation by metal oxides, often plays an important role in the overall dissipation and elimination of antibiotics in the environment. Several studies are available on the abiotic degradation of antibiotics [17–21], and all show substantial variation in the degradation rate.

* Corresponding author at: Key Laboratory of Soil Environment and Pollution Remediation, Institute of Soil Science, Chinese Academy of Sciences, Nanjing 210008, China. Tel.: +86 25 86881370; fax: +86 25 86881000.
E-mail address: zhaoling@issas.ac.cn (L. Zhao).
[1] Present address: Max Planck Institute for Marine Microbiology, Celsiusstrasse 1, D-28359 Bremen, Germany.

0304-3894/$ – see front matter © 2011 Elsevier B.V. All rights reserved.
doi:10.1016/j.jhazmat.2011.07.039

Manganese dioxide (MnO_2) is one of the most active and important oxidative components of soil systems, showing high potency in degrading various organic pollutants, such as substituted phenols and anilines, atrazine and antibacterial agents [18,19,22–24]. Abiotic degradation mediated by manganese minerals is an important transformational process of antibiotics in soil and aquatic environments. To our knowledge, the oxidation kinetics of tetracycline antibiotics by MnO_2 have been reported in previous studies [19,24], but the kinetics and products of CTC degradation have not yet been well described for MnO_2-oxidized reactions. Therefore, this study investigated transformation rates and possible products of CTC oxidized by δ-MnO_2 and the effect of different solutions on the transformation rates.

2. Materials and methods

2.1. Chemicals reagents

Chlortetracycline hydrochloride (97%) was purchased from Fluka (Milwaukee, WI, USA). Isochlortetracycline hydrochloride (I-CTC, 97%), anhydrochlortetracycline hydrochloride (A-CTC, 99%), 4-epichlortetracycline hydrochloride (E-CTC, 97%) and 4-epianhydrochlortetracycline hydrochloride (EA-CTC, 99%) were obtained from Sigma (New Jersey, USA). Ferulic acid (99%), *p*-coumaric acid (98%), caffeic acid (99%) and 2,6-dimethoxyphenol (99%) were purchased from Sigma–Aldrich (Milwaukee, WI, USA). All reagents were used in the same condition as they were received from the manufacturers. High-performance liquid chromatographic (HPLC)-grade methanol (MeOH) and acetonitrile (ACN) were purchased from Tedia (Fairfield, OH, USA). Ultra-pure water was obtained from Millipore Milli-Q Advantage A10 Water Purification System (Bedford, MA, USA). CTC stock solutions were prepared in MeOH to obtain a final concentration of 20 mM in a 15-mL amber borosilicate glass bottle with a brown screw cap. The bottles were protected from light and stored at −18 °C. The CTC stock solution was diluted with buffer solutions to constitute solutions with different concentrations on the day of experimental usage.

2.2. MnO_2 synthesis and characterization

MnO_2 was synthesized by the following method. Briefly stated, 200 mL of 35 g L^{-1} $KMnO_4$ was added drop-wise to 200 mL of 45 g L^{-1} $MnSO_4$ solution and mixed by a magnetic stirrer under neutral pH conditions. The precipitates were washed several times with Milli-Q water, and vacuum filtration was used for recovering the MnO_2 solids in each cycle. Additional washing was performed, if necessary, until no SO_4^{2-} was detected in the filtrate on testing by Ba^{2+}. The product was dried by heating at 103 °C for 12 h and then stored at 4 °C until further use. The synthesized MnO_2 was characterized as δ-MnO_2 by X-ray diffraction analysis (Fig. S1, supplementary material). The Brunauer–Emmett–Teller (BET)-specific surface area of δ-MnO_2 was determined to be 250 m^2 g^{-1} using a Micromeritics Tristar 3000 analyzer at −195 °C over a wide relative pressure range from 0 to 1. Scanning electron microscopy (SEM) images indicate that the synthesized δ-MnO_2 is composed of both granular and rod-shaped particles (Fig. S2, supplementary material). The pH_{zpc} (zero point of charge) for the synthesized MnO_2 was determined to be 2.3 in 0.1 mM NaCl solution by using a JS94H microiontophoresis apparatus (Shanghai, China).

2.3. Kinetic experiments

Batch reactions were conducted in 15-mL amber borosilicate glass bottles with brown screw caps and Teflon septa at 25 °C under constant shaking at 150 rpm. Reaction pH range of 3.0–6.0 was maintained with a 10 mM glacial acetic acid (HAc)–sodium acetate (NaAc) buffer system. Sodium chloride (NaCl) was added to adjust the ionic strength (I = 0.01 M). To exclude the influence of microbial effect on degradation, buffer solutions were sterilized at 130 °C for 30 min prior to use. MnO_2 solutions were prepared at concentrations of 50, 100, 150 and 200 mg L^{-1} by continuously stirring for at least 12 h on magnetic stirrers to homogenize the solution prior to use. CTC solutions were diluted to 200 μM with HAc–NaAc buffer from the stock solution. Five milliliters of δ-MnO_2 solution and CTC solution each were mixed together in 15-mL brown glass bottles for reactions and were duplicated. Reaction samples were periodically collected at time points from 3 min to 30 h. Two methods were used to quench the reaction: filtration through a 0.22-μm tetrafluoroethylene–perfluoropropylene filter, and the addition of 100 μL of 1 M oxalic acid to dissolve the remaining δ-MnO_2 particles. Besides this, the effect of temperature was studied by setting the reaction temperatures in the range of 15–35 °C.

The effect of pH was investigated by independently varying the buffer solutions. HAc–NaAc buffer was used to maintain pH < 6.0, while H_3BO_3–$Na_2B_4O_7$ buffer was used for pH > 7.0. Filtration method was used to quench reactions. Further, 2 mL of additional liquid samples were prepared to monitor the Mn^{2+} concentration during the reaction. Pure buffer with only CTC and pure buffer with only δ-MnO_2 were also set up as controls for the influence of the buffer solution on the reaction.

The effects of inorganic ions and organic substituted phenols were also investigated at pH 5.0 in buffer solutions with different concentrations of inorganic ions (K^+, Zn^{2+}, Ca^{2+}, Mg^{2+}, Al^{3+}, SO_4^{2-} and PO_4^{3-}) and organic substituted phenols (*p*-coumaric acid, ferulic acid, caffeic acid and 2,6-dimethoxyphenol). Reaction-quenching and sampling methods were the same as previously described.

2.4. Analysis of CTC and Mn^{2+}

CTC was analyzed by a 2695 Waters Alliance system (Milford, MA, USA) equipped with a diode-array UV/vis detector set to a wavelength of 360 nm. A Phenomenex Gemini C_{18} column (Torrance, CA, USA; 150 mm × 4.6 mm, 5 μm) was coupled to a Phenomenex Gemini C_{18} guard cartridge (4 mm × 3 mm). The column temperature was set at 40 °C. The HPLC mobile phase was a mixture of ACN and 1 mM oxalic acid at 18:82 (v/v) and was delivered at a flow rate of 1 mL min^{-1}. Each sample was analyzed twice, and the injection volume was 10 μL. Under these conditions, CTC had a retention time of 7.7 min.

The Mn^{2+} concentration generated was determined by an IRIS Advantage inductively coupled plasma (ICP) spectrometer with optical emission spectroscopy (OES) from Thermo Jarell Ash Company (USA). Controls with only MnO_2 and buffers but without CTC revealed that no dissolution of δ-MnO_2 occurred in the absence of CTC.

2.5. Product identification

In order to obtain sufficient amounts of all possible products for analysis, the initial concentrations of CTC and δ-MnO_2 were increased 10-fold, and two sets of 20 identical reactors were set up in parallel at pH 5.0. All reactors were quenched by centrifugation (4500 rpm × 15 min) after 72 h, and the supernatants as well as δ-MnO_2 solids were collected separately. The supernatants of all reactors were combined and extracted with Oasis-HLB solid-phase extraction tubes (1 mL) purchased from Waters (MA, USA). After extraction, products were eluted by 2 mL MeOH from the cartridge, and subsequently concentrated to 1 mL with a gentle N_2 gas stream. The products were then analyzed by LC–MS-MS. In a preliminary experiment, the δ-MnO_2 solids obtained were also washed

and extracted by MeOH. The extraction was concentrated and analyzed by HPLC. However, no measurable quantities of products could be detected by comparing with external standards, including CTC, I-CTC, E-CTC, A-CTC and EA-CTC. Thus, no further analysis of the possible products on the δ-MnO_2 surface was performed in this study.

The LC–MS-MS system (ThermoquestLCQ Duo, USA) was equipped with a Beta Basic-C_{18} HPLC column (150 mm × 2.1 mm i.d., 5 μm, Finnigan, Thermo, USA). The initial mobile phase (A) consisted of 200 mL MeOH and 310 μL formic acid in 1 L Milli-Q water. The second mobile phase (B) was prepared by mixing with 950 mL MeOH and 310 μL formic acid in 1 L Milli-Q water, by the method described by Søeborg et al. [25]. The gradient began at 95% A for 10 min, decreased rapidly to 50% A in 1 min, and was then maintained constantly at 50% A for 20 min. Then, it was increased to 95% A again in 1 min and held for 30 min to equilibrate the column. The flow rate was 0.2 mL min^{-1}. The MS was operated in the positive ion mode. The electrospray ionization (ESI) interface was selected and the capillary temperature was set to 300 °C with a voltage of 4 kV. The discharge current was 5 μA, and the sheath gas flow rate was 25 AU. Diagnostic fragment ions were obtained by the protonated molecule $[M+H]^+$, and ion signals were acquired by the time-scheduled, multiple-ion selected ion monitoring (SIM) mode. CTC, I-CTC, E-CTC, A-CTC and EA-CTC, as external standards, were analyzed by LC–MS-MS together with product samples using the same methods.

2.6. FTIR analysis

For Fourier transform-infrared (FTIR) spectroscopy, the δ-MnO_2 solids with CTC in the reactors as described above (Section 2.5) were collected by centrifugation (4500 rpm × 15 min) after 72 h. Control sample, just δ-MnO_2 in buffer solution without CTC, was also set up parallel and treated in the same way. The δ-MnO_2 slurries were re-suspended and washed in 15 mL Milli-Q-grade deionized water by gentle stirring and collected by centrifugation again. The slurries were then freeze-dried and stored at 35 °C for 2 days for further drying prior to analysis. The δ-MnO_2 solids (reacted and control samples) were analyzed by a NEXUS870 spectrometer from the Thermo Nicolet Company (Waltham, MA, USA) that was equipped with a photoacoustic detector (MTEC Photoacoustics Inc., Ames, IA, USA). The reference spectrum of untreated CTC standard was also acquired in the same analytical condition.

3. Results and discussion

3.1. CTC oxidative transformation kinetics

Fig. 1 presents a typical reaction profile at the condition of 0.01 M NaCl as background electrolyte, 25 °C and pH 5.0, where CTC concentration decreased and Mn^{2+} concentration increased as the reaction progressed. In the control experiment without δ-MnO_2, CTC was stable and no measurable loss was detected. However, a significant degradation of CTC occurred in the presence of δ-MnO_2. Mn^{2+} was generated and its concentration increased along with the reaction time. No Mn^{2+} was detected in the control experiment without CTC. The generation of Mn^{2+} shows that δ-MnO_2 was an oxidant in this system and CTC could be readily oxidized by δ-MnO_2. Although it is well known that CTC may chelate with divalent metal ion, no effect of the generated Mn^{2+} was observed on CTC quantification by complexation in this study, which has also been reported in previous studies [26,27].

To discover the role of adsorption in the reaction process, besides the filtration quenching method, oxalic acid was added to dissolve the residual δ-MnO_2 solid and quench the reaction as

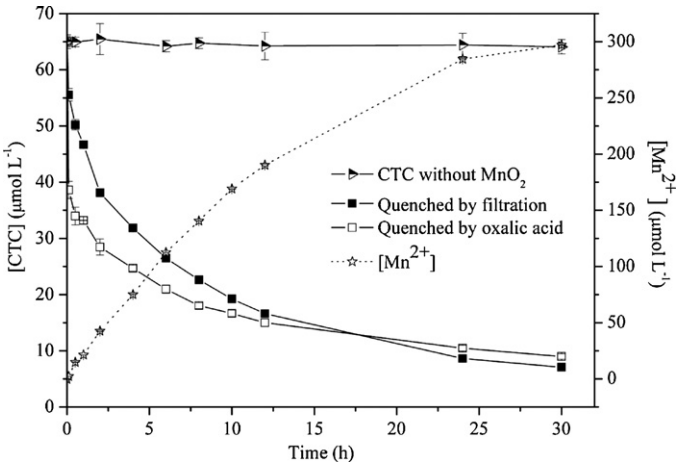

Fig. 1. The time courses of CTC oxidative transformation by δ-MnO_2 and generation of Mn^{2+} with 0.01 M NaCl as background electrolyte, at 25 °C and pH 5.0.

reported by Rubert and Pedersen [19]. The quenching time was approximately 7 s for the filtration quenching method and 30 s for the oxalic acid addition quenching method, which was determined by a preliminary experiment that no visible δ-MnO_2 particles could be found on a 0.22-μm tetrafluoroethylene–perfluoropropylene membrane after filtration at 30 s even when the amount of δ-MnO_2 was at a maximum value (100 mg L^{-1}) in this study. The residual CTC concentration quenched by oxalic acid was expected to be higher than that quenched by filtration. Contrary to expectation, the CTC concentrations in oxalic acid-quenched samples were lower than those in filtration samples collected prior to 12 h (Fig. 1). This was also observed in experiments with different initial δ-MnO_2 concentrations quenched by oxalic acid addition in this study (Fig. S3, supplementary material). Zhang et al. [24] also reported similar experimental phenomena wherein only negligible amounts of adsorbed CTC (about 1%) could be detected on the MnO_2 surface. Two reasons might generate this result wherein no considerable amount of adsorbed CTC is observed. One is that the time expended in dissolving the remaining δ-MnO_2 might result in some CTC loss during analysis; another reason could be that the pH in the system decreased rapidly after oxalic acid addition, thereby promoting a CTC transformation in the δ-MnO_2 system (Section 3.2). This result also implies that the adsorption rate of CTC on the δ-MnO_2 surface was lower than the rate of the oxidation step, which indicates that the adsorption was a rate-limiting step, by contrast to electron transfer between CTC and δ-MnO_2, according to the kinetic surface reaction model proposed by Stone [28] and Zhang et al. [24].

The pseudo-first-order kinetic model has been applied in previous investigations to evaluate the initial reaction kinetics of organic compounds with MnO_2 [29–31]; however, departure from the pseudo-first-order kinetics over the course of reactions has also been reported simultaneously. For better predicting long-term kinetics of organic compound oxidized by MnO_2, Rubert and Pedersen [19] applied a rate-retarded equation to fit OTC degradation kinetics by MnO_2 and a retarded factor (α) was used to describe the extent of departure from the pseudo-first-order behavior. Zhang et al. [24] also proposed a mechanism-based model to fit TCs degradation kinetics by MnO_2. In this study, the oxidation kinetics of CTC by δ-MnO_2 were tentatively fitted to these three kinetic models described above as well as to the pseudo-second-order kinetic model. As shown in Fig. S4 (supplementary material), the pseudo-second-order kinetic model was the best model for fitting the reaction kinetics among the four kinetic models, followed by the empirical rate-retarded equation and the pseudo-first-order kinetic model. The model least suited, based on the corresponding

Table 1
Summary of the apparent rate constant k_{obs} for CTC simulated by the pseudo-second-order kinetic model under different solution conditions.[a]

T (°C)	pH	[δ-MnO]$_0$ (mg L^{-1})	[CTC]$_0$ (μM)	$k_{obs} \times 10^{-3}$ (μM^{-1} h^{-1})	R^2
25	5.02	25	65	1.9 ± 0.1	0.97
25	5.02	50	65	3.5 ± 0.7[b]	0.99
25	5.02	50	65	3.2 ± 0.2[c]	0.99
25	5.02	75	65	7.0 ± 0.2	0.99
25	5.02	100	65	10.4 ± 0.5	0.97
25	5.02	50	18	24.1 ± 1.9	0.94
25	5.02	50	33	15.9 ± 0.6	0.98
25	5.02	50	65	3.5 ± 0.7	0.99
25	5.02	50	120	1.0 ± 0.1	0.96
25	3.77	50	65	37.5 ± 1.6	0.99
25	4.10	50	65	22.3 ± 1.2	0.99
25	5.02	50	65	3.5 ± 0.7	0.99
25	5.92	50	65	1.4 ± 0.2	0.96
25	7.41	50	65	0.2 ± 0.0	0.97
15	5.02	50	65	2.7 ± 0.1	0.97
25	5.02	50	65	3.5 ± 0.7	0.99
35	5.02	50	65	7.6 ± 0.2	0.99

[a] Significant at the 95% confidence level.
[b] Obtained using the filtration method for quenching the reaction.
[c] Obtained using the oxalic acid method for quenching the reaction.

R^2 values in Fig. S4 (supplementary material), for fitting reaction kinetics was the mechanism-based model by Zhang et al. [24], which was probably because the reaction kinetic data collected in this study (as shown in Fig. S3, supplementary material) were not completed enough to reach the request of the mechanism-based model, since this model strongly relies on completed reaction kinetics data collection, especially the later stage. On the other hand, the reaction kinetic constant (k_{obs}) values simulated by the empirical rate-retarded equation and the mechanism-based model by Zhang et al. [24] both exhibited inconsistent transformation trends of CTC compared with the corresponding experimental transformation rate curves under different reaction conditions, such as variable initial concentration of MnO_2 and CTC, pH and temperature, as shown in Tables S1 and S2 (supplementary material), respectively. Therefore, only the pseudo-second-order kinetic model was used to fit reaction kinetics under different conditions, and the rate constants (k_{obs}) under various conditions are listed in Table 1.

Rate constants of reaction increased rapidly with an increase in initial δ-MnO_2 concentrations. This accords well with the kinetic surface reaction model applied in previous studies on the oxidation of substituted phenols, substituted anilines and antibacterial agents by manganese oxides [18,19,28,29]. The increase in initial concentration of δ-MnO_2 can supply more active surface sites for more precursor complex formation, which could, in turn, increase the reaction rate. By contrast, the rate constants in reactions decreased considerably with an increase in initial CTC concentration when the concentration of MnO_2 was constantly maintained at 50 mg L^{-1}. A similar result was observed for CTC by Zhang et al. [24]. As the initial concentration of CTC increased further, the molar ratio of MnO_2 surface sites to CTC decreased, thus slowing down the rate of CTC adsorption on MnO_2 surface and finally reducing the rate constants.

3.2. Effect of pH

Both the degradation rate of CTC and the amount of Mn^{2+} yielded decreased significantly with an increase in pH (Fig. S5a and b, supplementary material), suggesting that an increase in pH could inhibit CTC transformation in MnO_2 system, which was supported by the k_{obs} of CTC in Table 1. Previous studies also confirmed that pH plays an important role in adsorption [33,34] and degradation [18,19,31] processes of antibiotics.

The pH of the solution influences not only the speciation of CTC (Fig. S6b, supplementary material) but also the surface-charge property and reduction potential of MnO_2 [31,32]. The speciation of CTC transits from cation to zwitterion and then to anion across the entire pH range (3.77–7.41) investigated because CTC has three distinct moieties, which correspond to tricarbonylamide (I), phenolic diketone (II) and dimethylamine (III), presented in Fig. S6a (supplementary material). Three pK_a values (pK_{a_1} = 3.30, pK_{a_2} = 7.44 and pK_{a_3} = 9.27) were reported for the tricarbonylamide (C1–C3), phenolic diketone (C10–C12) and dimethylamine (C4) moieties, respectively [35]. When pH was <3.30, the dimethylamine moiety carried a positive charge at the position of the nitrogen atom, while the other two moieties were neutral (Fig. S6b, supplementary material), which caused the CTC to exist mainly as a cation (CTC^{+00}). The enolic group of the tricarbonylamide moiety disassociated into an anion in the pH range 3.30–7.44. Thus, the zwitterionic form of CTC (CTC^{+-0}) became the dominant species with decreasing amounts of CTC^{+00}. The enolic groups at C10 and C12 (Fig. S6a) of the phenolic diketone moiety began to disassociate as anions at pH > 7.44, and CTC mainly existed in a negative form (CTC^{+--}). When pH increased over 9.27, the dimethylamine moiety became neutral and the other two moieties disassociated into anions. Thus, the negative ion CTC^{0--} was the dominant species. On the other way, the δ-MnO_2 particle was negatively charged under all tested pH conditions since its pH_{pzc} value was determined to be 2.3. The positively charged CTC moieties could be adsorbed at the negatively charged δ-MnO_2 surface via electrostatic force and the neutral CTC groups via the van der Waals interactions. Therefore, the adsorption of CTC at the MnO_2 surface declined because the negatively charged CTC species and the charge density of the MnO_2 surface increased with the increase of pH. Further, the tricarbonylamide moiety of CTC was less likely to be adsorbed onto the MnO_2 surface because of its negative charge under all tested pH levels. Phenolic diketone and dimethylamine were, therefore, expected to be active sites for CTC adsorption and oxidation on the MnO_2 surface. This is consistent with the oxidative products of CTC detected by LC–MS-MS (Section 3.6).

3.3. Effect of temperature

Temperature had a significant effect on the rate constants (k_{obs}) of CTC (Table 1). With an increase in temperature from 15 to 35 °C, the k_{obs} increased from 0.0027 to 0.0076 μM^{-1} h^{-1}, thereby

indicating an endothermic reaction. Its apparent activation energy for CTC transformation was estimated to be $45 \pm 14\,kJ\,mol^{-1}$ by fitting the rate constants obtained at various temperatures to the Arrhenius equation. The apparent activation energy of CTC in this study is lower than that of OTC ($60 \pm 2\,kJ\,mol^{-1}$) reported by Rubert and Pedersen [19]. This is in agreement with the result reported by Rubert and Pedersen [19] that the reactivity of CTC is higher than that of OTC oxidized by MnO_2.

3.4. Effect of inorganic ions

Coupled with the oxidation of CTC, Mn^{2+} was generated by reduction of δ-MnO_2. The generated Mn^{2+} could be adsorbed on the negatively charged MnO_2 surface, thereby slowing reaction rates. This inhibitory effect has been documented for MnO_2-oxidized reactions for phenols, anilines and antimicrobial agents [23,31]. To quantify such an effect on CTC transformation, a series of experiments were performed by adding metal ions and anions to the reaction systems at pH 5.0. The resulting k_{obs} values are summarized in Table 2. The table clearly shows that the addition of Mn^{2+} and Zn^{2+} considerably decreased the transformation rate of CTC oxidation by δ-MnO_2. The presence of low concentrations (at 10% MnO_2 initial concentration) of Mn^{2+} and Zn^{2+} ions decreased the rate of reaction by 37% and 29%, respectively. Further, the inhibition effect increased remarkably in a nonlinear manner as the additional Mn^{2+} concentration increased. At background Mn^{2+} concentrations of 57.5 and 287.5 μM, the k_{obs} value decreased by 37% and 66%, respectively. Compared with Mn^{2+} and Zn^{2+}, no pronounced inhibition effect was observed with the addition of four other metal ions (K^+, Mg^{2+}, Ca^{2+} and Al^{3+}) and two anions (SO_4^{2-} and PO_4^{3-}). The two anions were less likely to adsorb on the δ-MnO_2 surface due to repulsive forces; however, the lack of an inhibition effect of the addition of four metal ions on the transformation rate suggested that these co-solutes did not compete with CTC for the same surface sites reported by Zhang and Huang [31] due to their weak sorption affinities on the δ-MnO_2 surface [36]. The inhibition effect of Zn^{2+} was caused only by its competition with CTC for occupation of the Mn^{4+} vacancy sites of the δ-MnO_2 layers, but not by its reaction with Mn^{4+} for lowering the average oxidation state of δ-MnO_2 [37,38]. However, the greater inhibition effect of Mn^{2+}, besides its occupation of the reaction sites of the δ-MnO_2 layers as similar as Zn^{2+}, might be primarily attributed to competing with CTC for its reduction of Mn^{4+} of δ-MnO_2 and hence to lowering the average oxidation state of δ-MnO_2 [38,39].

3.5. Effect of substituted phenols

Substituted phenols, such as *p*-coumaric acid, ferulic acid, caffeic acid and 2,6-dimethoxyphenol, are widely distributed in natural soil and aquatic environments. Previous studies have reported that the phenolic groups of these substituted phenols could affect the reaction efficiency of chlorophenols and sulfonamide antimicrobials via cross-coupled reactions in the presence of phenoloxidases or acid birnessite [22,40]. In this study, several substituted phenols were chosen as simple models to determine the effect of the organic matter on CTC oxidative transformation by MnO_2. A series of experiments were performed by adding different substituted phenols to the reaction solutions at pH 5.0. The resulting k_{obs} are listed in Table 3. The *t* values in Table 3 obtained by *T*-test were all over 3.792 ($t_{0.001,22} = 3.792$), indicating that the addition of substituted phenols could significantly decrease the CTC transformation rate. The inhibition effect also increased considerably as the *p*-coumaric acid concentration increased, although not in a directly proportional manner. The addition of the same concentrations (100 μM) of *p*-coumaric acid, ferulic acid, caffeic acid and 2,6-dimethoxyphenol decreased CTC transformation rate by 80, 97, 36 and 43%, respectively. Likewise, the k_{obs} values of *p*-coumaric acid, ferulic acid, caffeic acid and 2,6-dimethoxyphenol alone with MnO_2 were 3.9 ± 0.1, 1271.4 ± 72.3, 15.5 ± 0.6 and $145.2 \pm 2.4\,\mu M^{-1}\,h^{-1}$ in Table 3, respectively. It is clear that the inhibition effect of substituted phenols on CTC transformation rate was consistent with its reaction capacity with MnO_2 except *p*-coumaric acid. This result indicates that the inhibition effect of these substituted phenols was primarily attributed to competing with CTC to react with MnO_2. Comparing the molecular structures of four substituted phenols (Fig. S7, supplementary material), at *ortho*-position of phenolic group, only *p*-coumaric acid has no substituent, suggesting that *p*-coumaric acid might be more favorable to adsorb on MnO_2 surfaces than the other three substituted phenols due to its lower steric hindrance on MnO_2 surfaces. Thereby, the strong sorption affinity of *p*-coumaric acid might offset the weak reaction capacity with MnO_2, which resulted in the greater inhibition effect on CTC transformation rate of *p*-coumaric acid than that of caffeic acid and 2,6-dimethoxyphenol.

Table 2
Effect of background ions on the apparent rate constant k_{obs} for CTC simulated by the pseudo-second-order kinetic model.[a]

Addition of ion	$[Ion]_0$ (μmol L^{-1})	$k_{obs} \times 10^{-3}$ ($\mu M^{-1}\,h^{-1}$)[b]	R^2
Control reactor	0	3.5 ± 0.7	0.99
	5.75	3.6 ± 0.1	0.99
Mn^{2+}	57.5	2.3 ± 0.1	0.99
	287.5	1.3 ± 0.0	0.99
Zn^{2+}	57.5	2.5 ± 0.1	0.99
K^+	57.5	3.3 ± 0.1	0.99
Ca^{2+}	57.5	3.5 ± 0.1	0.99
Mg^{2+}	57.5	4.1 ± 0.1	0.99
Al^{3+}	57.5	3.5 ± 0.1	0.99
SO_4^{2-}	57.5	3.6 ± 0.1	0.99
PO_4^{3-}	57.5	3.3 ± 0.1	0.99

[a] Experimental conditions: pH 5.02, $[CTC]_0 = 65$ μM, and $[\delta\text{-}MnO_2]_0 = 50$ mg L^{-1}.
[b] Significant at the 95% confidence level.

3.6. Oxidation products of CTC

With LC–MS-MS analysis, four products were confirmed via comparison with authentic standards and six other products were also tentatively identified on the basis of their mass spectra together with relevant reports on degradation products of TCs [25,41–43] since no commercially authentic standards are available. The SIM chromatograms and the individual MS^2 spectra of possible transformation products are presented in Fig. 2, and the chemical structures of these possible products are depicted in Fig. 3.

Two product ions at *m*/*z* 462 were obtained from the precursor ions with *m*/*z* 479, corresponding to I-CTC $[I\text{-}CTC\text{-}H]^+$ ($t_R = 6.36$ min) and E-CTC $[E\text{-}CTC\text{-}H]^+$ ($t_R = 10.07$ min). These products were identified and confirmed with the standard values under the same analysis conditions by LC–MS-MS. CTC can be converted to I-CTC under alkaline conditions, while E-CTC has been found to be formed in acidic solutions in a pH range from 2 to 6 [44]. The bond between C6 and C11a atoms (Fig. S6a, supplementary material) could be disrupted as a consequence of the catalyzation by intramolecular cyclization of the hydroxyl moiety of the MnO_2 surface to yield I-CTC at pH 5.0, as noted in this study. Meanwhile, CTC could easily epimerize at position C4 to form E-CTC [45]. Thus, I-CTC and E-CTC may be considered as byproducts of CTC reactions in the presence of MnO_2 at pH 5.0.

Two additional product ions at *m*/*z* 462 were also obtained from the precursor ions with *m*/*z* 479, which were tentatively characterized as keto-CTC $[K\text{-}CTC\text{-}H]^+$ ($t_R = 10.07$ min) and 4-epi-keto-CTC $[EK\text{-}CTC\text{-}H]^+$ ($t_R = 8.92$ min), respectively, based on fragmentation pattern of their MS^2 spectra, with regard to the structures and conditions of formation for K-CTC and EK-CTC that were proposed

Table 3
Effect of substituted phenols on the apparent rate constant k_{obs} for CTC simulated by the pseudo-second-order kinetic model.[a]

Substituted phenol (SP)	$[SP]_0$ (μM)	$[CTC]_0$ (μM)	$k_{obs} \times 10^{-3}$ ($\mu M^{-1} h^{-1}$)[b]		R^2	t[d]
			CTC	SP[c]		
Control	0	65	3.5 ± 0.7		0.99	
p-Coumaric acid	50	65	1.7 ± 0.0		0.99	8.9
	50	0		10.1 ± 0.5	0.98	
	100	65	0.7 ± 0.0		0.97	13.7
	100	0		3.9 ± 0.1	0.99	
	200	65	0.3 ± 0.0		0.95	15.5
	200	0		0.8 ± 0.1	0.95	
Ferulic acid	100	65	0.1 ± 0.0		0.97	13.7
	100	0		1271.4 ± 72.3	0.99	
Caffeic acid	100	65	2.6 ± 0.1		0.99	4.3
	100	0		15.5 ± 0.6	0.95	
2,6-Dimethoxyphenol	100	65	2.0 ± 0.1		0.99	6.4
	100	0		145.2 ± 2.4	0.99	

[a] Experimental conditions: pH 5.02 and $[\delta\text{-}MnO_2]_0 = 50\ mg\ L^{-1}$.
[b] Significant at the 95% confidence level.
[c] The k_{obs} values of substituted phenols oxidized by δ-MnO_2 without CTC simulated by the pseudo-second-order kinetic model.
[d] t means T-test of the apparent rate constant under the presence of different substituted phenols (the degree of freedom = 22).

by Halling-Sørensen et al. [41], who reported that K-CTC could be reversibly formed from CTC at pH 3–9. Previous studies demonstrated that as solid, E-CTC and CTC exist as enol forms, but in aqueous solutions an equilibrium is formed between the keto and enol tautomers [46,47], indicating that K-CTC and EK-CTC can be generally thought as accompanied composition of CTC and E-CTC standard in solutions. Blanchflower et al. [48] further found that EK-CTC was formed rapidly in fresh acidic aqueous solutions of E-CTC, but K-CTC formed more slowly (over a period of days) from CTC due to the higher stability of CTC than E-CTC. Hence, although the identification of K-CTC and EK-CTC was not confirmed because of the absence of commercial standards, the generation of K-CTC and EK-CTC could be assured during the reaction of CTC with MnO_2 based on previous works described above. Additionally, characteristic fragment ions in the individual MS^2 spectra of E-CTC, K-CTC and EK-CTC contained the identical fragment ions, such as m/z 462 and 444, indicating that they might be isomers.

Product ions at m/z 444 were obtained from the precursor ions with m/z 461.9, corresponding to A-CTC (t_R = 22.80 min) and EA-CTC (t_R = 19.85 min), which have also been confirmed by the standard controls. Their MS^2 fragments with m/z 444 were derived by removing one molecule of NH_3 from A-CTC or EA-CTC. A-CTC and EA-CTC could be anticipated as predominant abiotic degradation products of CTC at pH 3–6.5 in the aqueous environment, as reported by Halling-Sørensen et al. [41]. A-CTC was formed via elimination of one H_2O molecule by losing a hydrogen atom at C5a and a hydroxyl group at C6 in a CTC molecule, and EA-CTC was the 4-epimer of A-CTC.

Two products contained molecular ions of m/z 451 ($[M+H]^+$) and the difference between the molecular weight of these two compounds and CTC was equal to 28, indicating the possibility of losing two methyl groups from CTC. Their MS^2 fragments with m/z 433, 434 and 416 corresponded to the daughter ions of $[M+H-H_2O]^+$, $[M+H-NH_3]^+$ and $[M+H-NH_3-H_2O]^+$ by loss of H_2O, NH_3 and $NH_3 + H_2O$ moieties from the molecular ion, respectively. Based on the molecular weight of the compounds and the fragmentation pattern, we suggested that these two compounds could be *N*-didemethyl products formed by the loss of two methyl groups from the dimethylamine moiety at the C4 position of CTC, which corresponded with *N*-didemethyl-CTC (*N*-DDM-CTC, t_R = 19.13 min) and 4-epi-*N*-didesmethyl-CTC (EN-DDM-CTC, t_R = 9.65 min). Similarly, the molecular ions of m/z 465 were tentatively considered the products of *N*-demethyl-CTC (*N*-DM-CTC, t_R = 21.98 min) and its 4-epimer (EN-DM-CTC, t_R = 20.07 min), with MS^2 fragments of m/z 448, 447, and 430 corresponding to the daughter ions of $[M+H-NH_3]^+$, $[M+H-H_2O]^+$ and $[M+H-NH_3-H_2O]^+$ by loss of NH_3, H_2O and $NH_3 + H_2O$, respectively. The demethyl products could, theoretically, also be formed by loss of a methyl group from the C6 position of CTC, such as 6-demethyl-CTC and its epimer corresponding to m/z 465, by comparison with *N*-DM-CTC and EN-DM-CTC proposed in this study. According to previous studies, 6-demethyl products could only be isolated as impurities from the bacterial production of TCs [49], which indicated that the formation of 6-DM-CTC was difficult through an abiotic degradation of CTC. Thus, we tentatively identified that the demethyl products were *N*-DM-CTC and *N*-DDM-CTC in the samples.

In addition to these 10 proposed products, certain other compounds with molecular ions at m/z 402, 432, 445, 447, 453, 456, 463, 466, 475, 511 and 525 could not be identified because neither commercial standards nor published information was available for analysis of their structures. Future research dedicated to the identification of these possible transformational products is needed.

3.7. FTIR analysis

FTIR spectroscopy was used to analyze the changes on δ-MnO_2 surface after reacting with CTC (Fig. 4). Peak assignments for non-reacted δ-MnO_2 (Fig. 4a) were referred to the study by Nakamoto [50]. The strong broad peak at 3393 cm^{-1} corresponded with the stretching vibration of the hydroxyl group in water and Mn–O–H molecules. The 1625 and 1085 cm^{-1} bands were assigned to the bending vibrations of the hydroxyl groups of Mn–OH, suggesting that δ-MnO_2 in this study is a hydrous manganese oxide containing numerous hydroxyl groups on the surface. The 528 cm^{-1} band was assigned to the bending vibration of Mn–O, indicating the presence of a crystal cell of MnO_2 molecule. Compared with the spectrum of non-reacted MnO_2, many peaks occurred between 1200 and 1800 cm^{-1} in the spectrum of MnO_2 that underwent reaction with CTC (Fig. 4b). These additional IR absorption peaks depicted in Fig. 4b are attributed to the most characteristic region of non-reacted CTC spectrum in Fig. 4c. Peak assignments for CTC in Fig. 4c concur with the report on the FTIR spectrum of TC [51,52]. The 1669 and 1518 cm^{-1} bands were assigned to the carbonyl and amino groups, respectively, of the amide in ring A (Fig. S6a, supplementary material). Frequencies at 1618 and 1577 cm^{-1} corresponded with the carbonyl groups in A and C rings, respectively. The

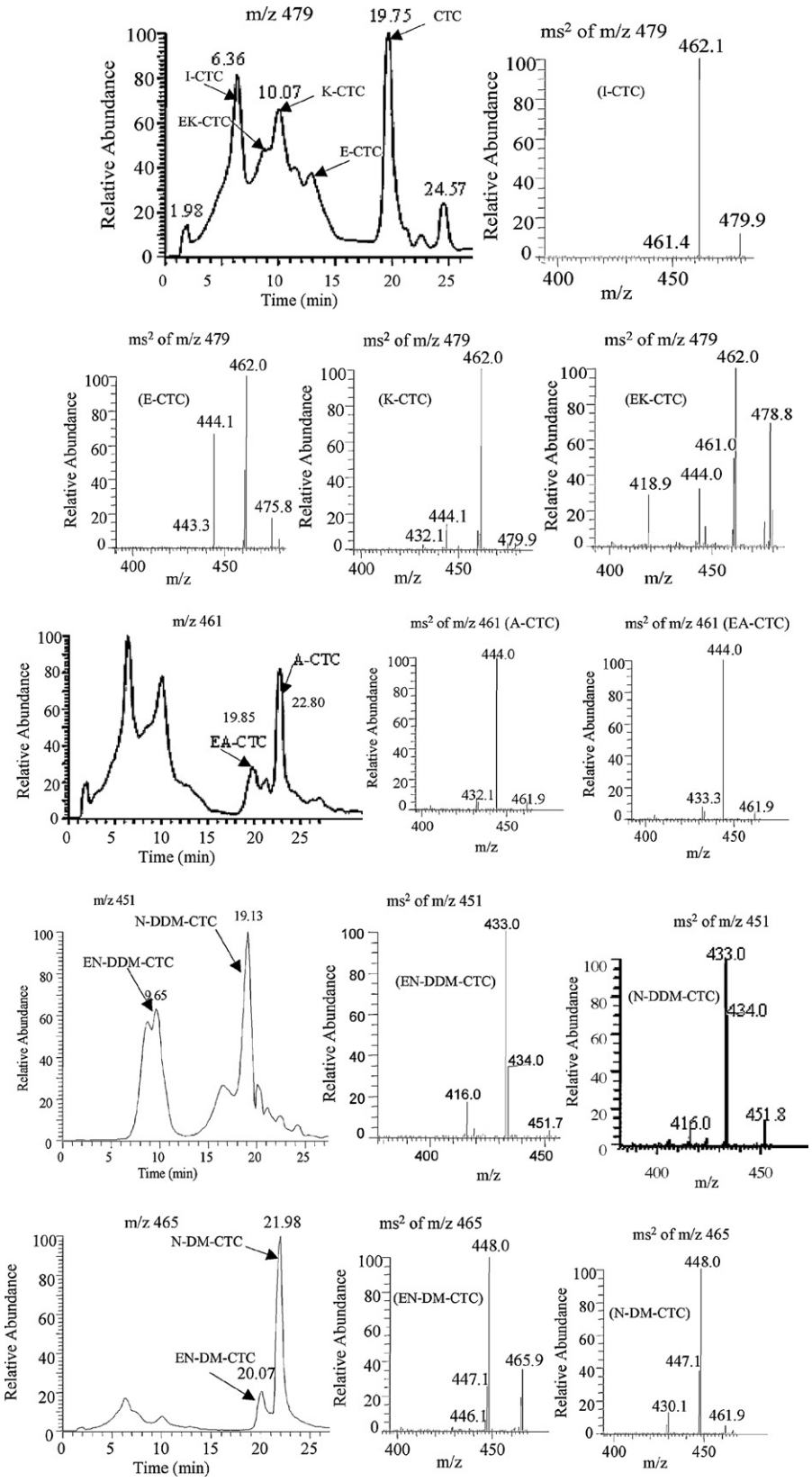

Fig. 2. SIM chromatograms presented with individual MS^2 spectra of possible transformational products of CTC by δ-MnO_2.

1505 and 1444 cm^{-1} bands were assigned to the aromatic amino moiety of the dimethylamine group and to the skeletal vibration, respectively. Although it was difficult to assign the band shift in the spectrum of CTC that reacted with MnO_2, the band changes of carbonyl, amide carbonyl and amino groups in ring A and carbonyl groups in ring C (Fig. 4b) were apparent. A shift in the carbonyl absorption band from 1669, 1618 and 1577 to 1600 cm^{-1} might be interpreted as the participation of carbonyl groups in hydrogen

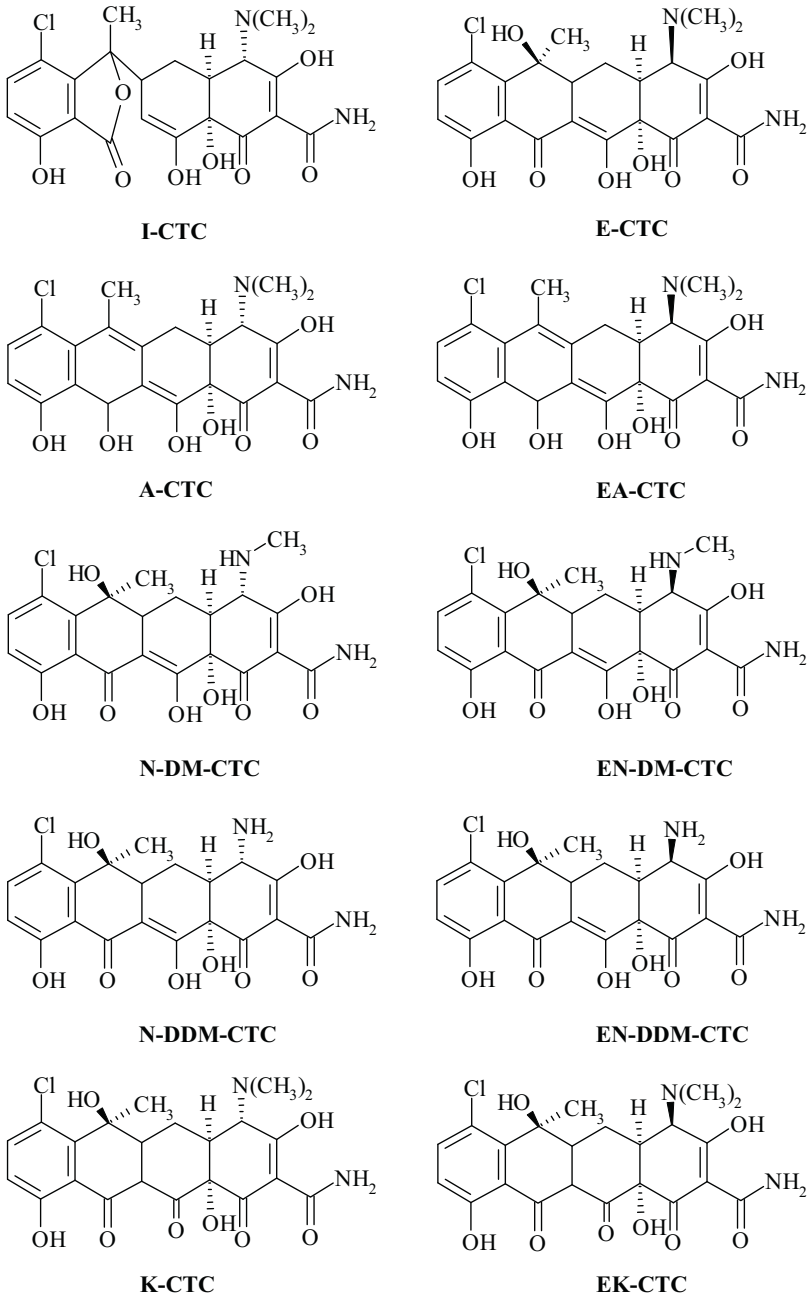

Fig. 3. Chemical structures of possible transformational products of CTC by δ-MnO_2.

bonding with hydroxyl groups on the surface of MnO_2 or as coordination of carbonyl groups with Mn^{4+} on the surface of MnO_2 [53]. A shift of the amide absorption band from 1505 to 1484 cm^{-1} indicated participation of amide at the C4 position functioned with MnO_2. Further, a band loss of Mn–OH or a clear shift of Mn–OH adsorption band at 1625 and 1085 cm^{-1} in Fig. 4b indicates that numerous Mn–OH groups on the MnO_2 surface might be active sites for CTC adsorption and oxidation based on the FTIR result.

3.8. Environmental significance

According to this study, CTC could be rapidly degraded by MnO_2, indicating that MnO_2 in the environment will facilitate transformation of tetracycline antibiotics. The risk of CTC contamination in agricultural soil still exists because of its extensive usage, despite the fact that appropriate compost methods are available to reduce the amount of CTC residue in livestock manure, which presents a great potential for release into the environment [54,55]. Considering the effect of pH on CTC oxidative degradation in the presence of MnO_2, the transformation of CTC will be accelerated when the manure contaminated with CTC is used as fertilizer in some weakly acidic soils. Furthermore, the reaction products revealed that oxidative transformation of CTC by MnO_2 could reduce its toxicity on microorganisms because the degradation products were generally found to be less toxic than their parental compound, except for A-CTC and EA-CTC, according to their MIC_{50} and EC_{50} values reported by Halling-Sørensen et al. [41]. A-CTC and EA-CTC belong to the “atypical tetracyclines”, which have a different mode of action compared to the parental compounds [56]. They interfere with membrane permeability and may exhibit activity

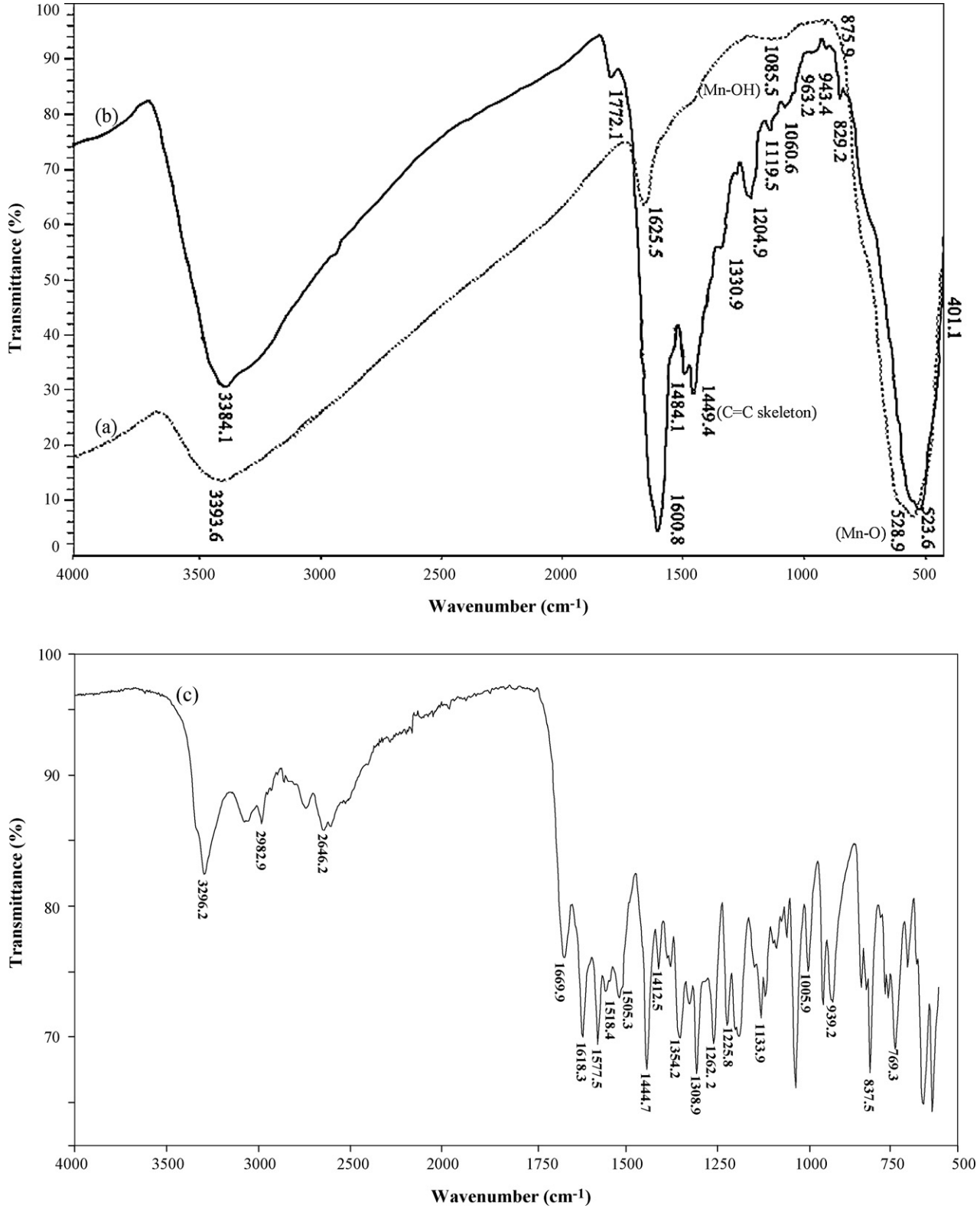

Fig. 4. FTIR spectra of (a) δ-MnO_2 and (b) δ-MnO_2 reaction with CTC; (c) CTC at pH 5.0.

against organisms that are resistant to CTC. No literature can be found to compare the toxicities of *N*-demethylation products of CTC with that of the parent compound. The antimicrobial activity of these demethylation products of CTC necessitates further investigation.

4. Conclusion

CTC was proved to be efficiently degraded by δ-MnO_2. The measured CTC transformation rates increased with an increase in the initial concentration of δ-MnO_2 and reaction temperature;

however, transformation rates decreased with an increase in the initial CTC concentration and pH. The addition of metal ions (Mn^{2+} and Zn^{2+}) and substituted phenols can reduce transformation rates of CTC by competitive inhibition of adsorption on δ-MnO_2 surfaces or reaction with δ-MnO_2, respectively. Isomerization, dehydration, cyclization, ketonization and *N*-demethylation products were evaluated by LC–MS-MS analysis, which indicated that the hydroxyl groups at C6 and C12 and the dimethylamine moiety were the active sites for CTC reaction with the Mn–OH moieties on the MnO_2 surface. The formation of less toxic products implies that the abiotic transformation of CTC by MnO_2 is likely to minimize the environmental risk constituted by CTC discharged into the environment.

Acknowledgements

This work was funded by the Major State Basic Research Development Program (2007CB936604), the National Natural Science Foundation of China (20707029 and 40671093), the Natural Scientific and Technical Supporting Program (2006BAD10B05), and the Innovation Project of Chinese Academy of Sciences (KSCX2-YW-N-51-02). Sincere thanks go to Ulrike Jaekel from the Max Planck Institute for Marine Microbiology, Bremen, Germany for English language revision of the manuscript and helpful comments.

Appendix A. Supplementary data

Supplementary data associated with this article can be found, in the online version, at doi:10.1016/j.jhazmat.2011.07.039.

References

[1] A.K. Sarmah, M.T. Meyer, A.B.A. Boxall, A global perspective on the use, sales, exposure pathways, occurrence, fate and effects of veterinary antibiotics (VAs) in the environment, Chemosphere 65 (2006) 725–759.
[2] V. Calisto, V.I. Esteves, Psychiatric pharmaceuticals in the environment, Chemosphere 77 (2009) 1257–1274.
[3] D.J. Yu, X.L. Yi, Y.F. Ma, B. Yin, H.L. Zhuo, J. Li, Y.F. Huang, Effects of administration mode of antibiotics on antibiotic resistance of *Enterococcus faecalis* in aquatic ecosystems, Chemosphere 76 (2009) 915–920.
[4] S. Kim, H.K. Park, K. Chandran, Propensity of activated sludge to amplify or attenuate tetracycline resistance genes and tetracycline resistant bacteria: a mathematical modeling approach, Chemosphere 78 (2010) 1071–1077.
[5] M.H.M.M. Montforts, D.F. Kalf, P.L.A. van Vlaardingen, J.B.H.J. Linders, The exposure assessment for veterinary medicinal products, Sci. Total Environ. 225 (1999) 119–133.
[6] D.W. Kolpin, E.T. Furlong, M.T. Meyer, E.M. Thurman, S.D. Zaugg, L.B. Barber, H.T. Buxton, Pharmaceuticals, hormones and other organic wastewater contaminants in US streams 1999–2000: a national reconnaissance, Environ. Sci. Technol. 36 (2002) 1202–1211.
[7] A.B.A. Boxall, L.A. Fogg, P.A. Blackwell, P. Kay, E.J. Pemberton, A. Croxford, Veterinary medicines in the environment, Rev. Environ. Contam. Toxicol. 180 (2004) 1–91.
[8] T. Tylová, J. Olšovská, P. Novák, M. Flieger, High-throughput analysis of tetracycline antibiotics and their epimers in liquid hog manure using Ultra Performance Liquid Chromatography with UV detection, Chemosphere 78 (2010) 353–359.
[9] G. Hamscher, S. Sczesny, H. Höper, H. Nau, Determination of persistent tetracycline residues in soil fertilized with liquid manure by high-performance liquid chromatography with electrospray ionization tandem mass spectrometry, Anal. Chem. 74 (2002) 1509–1518.
[10] G. Hamscher, H.T. Pawelzick, H. Höper, H. Nau, Different behaviour of tetracyclines and sulfonamides in sandy soils after repeated fertilisation with liquid manure, Environ. Toxicol. Chem. 24 (2005) 861–868.
[11] K. Kumar, A. Thompson, A.K. Singh, Y. Chander, S.C. Gupta, Enzyme-linked immunosorbent assay for ultratrace determination of antibiotics in aqueous samples, J. Environ. Qual. 33 (2004) 250–256.
[12] N. Kemper, Veterinary antibiotics in the aquatic and terrestrial environment, Ecol. Indicators 8 (2008) 1–13.
[13] A. Katayama, R. Bhula, G.R. Burns, E. Carazo, A. Felsot, D. Hamilton, C. Harris, Y.H. Kim, G. Kleter, W. Koerdel, J. Linders, J.G.M.W. Peijnenburg, A. Sabljic, R.G. Stephenson, D.K. Racke, B. Rubin, K. Tanaka, J. Unsworth, R.D. Wauchope, Bioavailability of xenobiotics in the soil environment, Rev. Environ. Contam. Toxicol. 203 (2010) 1–86.
[14] B. Halling-Sørensen, A.M. Jacobsen, J. Jensen, G. Sengelov, E. Vaclavik, F. Ingerslev, Dissipation and effects of chlortetracycline and tylosin in two agricultural soils: a field-scale study in southern Denmark, Environ. Toxicol. Chem. 24 (2005) 802–810.
[15] O.B. Samuelsen, B.T. Lunestad, A. Ervik, S. Fjelde, Stability of antibacterial agents in an artificial marine aquaculture sediment studied under laboratory conditions, Aquaculture 126 (1994) 283–290.
[16] R. Alexy, T. Kümpel, K. Kümmerer, Assessment of degradation of 18 antibiotics in the closed bottle test, Chemosphere 57 (2004) 505–512.
[17] H. Oka, Y. Ikai, N. Kawamura, M. Yamada, K. Harada, S. Ito, M. Suzuki, Photodecomposition products of tetracycline in aqueous solution, J. Agric. Food Chem. 37 (1989) 226–231.
[18] H.C. Zhang, C.H. Huang, Oxidative transformation of fluoroquinolone antibacterial agents and structurally related amines by manganese oxide, Environ. Sci. Technol. 39 (2005) 4474–4483.
[19] K.F. Rubert, J.A. Pedersen, Kinetics of oxytetracycline reaction with a hydrous manganese oxide, Environ. Sci. Technol. 40 (2006) 7216–7221.
[20] W.R. Chen, C.H. Huang, Adsorption and transformation of tetracycline antibiotics with aluminum oxide, Chemosphere 79 (2010) 779–785.
[21] J.S. Jeong, W.H. Song, W.J. Cooper, J.Y. Jung, J. Greaves, Degradation of tetracycline antibiotics: mechanisms and kinetic studies for advanced oxidation/reduction processes, Chemosphere 78 (2010) 533–540.
[22] J.W. Park, J. Dec, J.E. Kim, J.M. Bollag, Effect of humic constituents on the transformation of chlorinated phenols and anilines in the presence of oxidoreductive enzymes or birnessite, Environ. Sci. Technol. 33 (1999) 2028–2034.
[23] J.Y. Shin, M.A. Cheney, Abiotic transformation of atrazine in aqueous suspension of four synthetic manganese oxides, Colloids Surf. A 242 (2004) 85–92.
[24] H.C. Zhang, W.R. Chen, C.H. Huang, Kinetic modeling of oxidation of antibacterial agents by manganese oxide, Environ. Sci. Technol. 42 (2008) 5548–5554.
[25] T. Søeborg, F. Ingerslev, B. Halling-Sørensen, Chemical stability of chlortetracycline and chlortetracycline degradation products and epimers in soil interstitial water, Chemosphere 57 (2004) 1515–1524.
[26] J.J. Morgan, Kinetics of reaction between O_2 and Mn (II) species in aqueous solutions, Geochim. Cosmochim. Acta 69 (2004) 35–48.
[27] W.R. Chen, C.H. Huang, Transformation of tetracyclines mediated by Mn (II) and Cu (II) ions in the presence of oxygen, Environ. Sci. Technol. 43 (2009) 401–407.
[28] A.T. Stone, Reductive dissolution of manganese (III/IV) oxides by substituted phenols, Environ. Sci. Technol. 21 (1987) 979–988.
[29] S. Laha, R.G. Luthy, Oxidation of aniline and other primary aromatic amines by manganese dioxide, Environ. Sci. Technol. 24 (1990) 363–373.
[30] J. Klausen, S.B. Haderlein, R.P. Schwarzenbach, Oxidation of substituted anilines by aqueous MnO_2: effect of co-solutes on initial and quasi-steady-state kinetics, Environ. Sci. Technol. 31 (1997) 2642–2649.
[31] H.C. Zhang, C.H. Huang, Oxidative transformation of triclosan and chlorophene by manganese oxides, Environ. Sci. Technol. 37 (2003) 2421–2430.
[32] R.A. Petrie, P.R. Grossl, R.C. Sims, Oxidation of pentachlorophenol in manganese oxide suspensions under controlled E_h and pH environments, Environ. Sci. Technol. 36 (2002) 3744–3748.
[33] J. Gao, J.A. Pedersen, Adsorption of sulfonamide antimicrobial agents to clay minerals, Environ. Sci. Technol. 39 (2005) 9509–9516.
[34] M.E. Parolo, M.C. Savini, J.M. Vallés, M.T. Baschini, M.J. Avena, Tetracycline adsorption on montmorillonite: pH and ionic strength effects, Appl. Clay Sci. 40 (2008) 179–186.
[35] C.R. Stephens, K. Murai, K.J. Brunings, R.B. Woodward, Acidity constants of the tetracycline antibiotics, J. Am. Chem. Soc. 78 (1956) 4155–4158.
[36] J.W. Tonkin, L.S. Balistrieri, J.W. Murray, Modeling sorption of divalent metal cations on hydrous manganese oxide using the diffuse double layer model, Appl. Geochem. 19 (2004) 29–53.
[37] B. Toner, A. Manceau, S.M. Webb, G. Sposito, Zinc sorption to biogenic hexagonal-birnessite particles within a hydrated bacterial biofilm, Geochim. Cosmochim. Acta 70 (2006) 27–43.
[38] A. Manceau, B. Lanson, V.A. Drits, Structure of heavy metal sorbed birnessite. Part III: Results from powder and polarized extended X-ray absorption fine structure spectroscopy, Geochim. Cosmochim. Acta 66 (2002) 2639–2663.
[39] J.L. Junta, M.F. Hochella Jr., Manganese (II) oxidation at mineral surfaces: a microscopic and spectroscopic study, Geochim. Cosmochim. Acta 58 (1994) 4985–4999.
[40] H.M. Bialk, A.J. Simpson, J.A. Pedersen, Cross-coupling of sulfonamide antimicrobial agents with model humic constituents, Environ. Sci. Technol. 39 (2005) 4463–4473.
[41] B. Halling-Sørensen, G. Sengeløv, J. Tjørnelund, Toxicity of tetracyclines and tetracycline degradation products to environmentally relevant bacterial, including selected tetracycline-resistant bacterial, Arch. Environ. Contam. Toxicol. 42 (2002) 263–271.
[42] B. Halling-Sørensen, A. Lykkeberg, F. Ingerslev, P. Blackwell, J. Tjørnelund, Characterisation of the abiotic degradation pathways of oxytetracyclines in soil interstitial water using LC–MS-MS, Chemosphere 50 (2003) 1331–1342.
[43] J. Diana, L. Vandenbosch, B. De Spiegeleer, J. Hoogmartens, E. Adams, Evaluation of the stability of chlortetracycline in granular premixes by monitoring its conversion into degradation products, J. Pharm. Biomed. Anal. 39 (2005) 523–530.
[44] L.A. Mitscher, The Chemistry of the Tetracycline Antibiotics Medicinal Research Series, vol. 9, Marcel Dekker, New York, 1978.
[45] D.A. Hussar, P.J. Niebergall, E.T. Sugita, J.T. Doluisio, Aspects of the epimerization of certain tetracycline derivatives, J. Pharm. Pharmacol. 20 (1968) 539–546.
[46] P.D. Bryan, K.R. Hawkins, J.T. Stewart, A.C. Capomacchia, Analysis of chlortetracycline by high performance liquid chromatography with postcolumn

alkaline-induced fluorescence detection, Biomed. Chromatogr. 6 (1992) 305–310.
[47] W. Naidong, R. Roets, R. Busson, J. Hoogmartens, Separation of keto-enol tautomers of chlortetracycline and 4-epichlortetracycline by liquid chromatography on poly(styrene–divinylbenzene) copolymer, J. Pharm. Biomed. Anal. 8 (1990) 881–889.
[48] W.J. Blanchflower, R.J. McCracken, A.S. Haggan, D.G. Kennedy, Confirmatory assay for the determination of tetracycline, oxytetracycline, chlortetracycline and its isomers in muscle and kidney using liquid chromatography–mass spectrometry, J. Chromatogr. B: Biomed. Sci. Appl. 692 (1997) 351– 360.
[49] J.R.D. McCormick, N.O. Sjolander, U. Hirsch, E.R. Jensen, A.P. Doerschuk, A new family of antibiotics: the demethyl-tetracyclines, J. Am. Chem. Soc. 79 (1957) 4561–4563.
[50] K. Nakamoto, Infrared and Raman Spectra of Inorganic and Coordination Compound, third ed., John Wiley, New York, 1978.
[51] C. Gu, K.G. Karthikeyan, Interaction of tetracycline with aluminum and iron hydrous oxides, Environ. Sci. Technol. 39 (2005) 2660–2667.
[52] Y. Wan, Y.Y. Bao, Q.X. Zhou, Simultaneous adsorption and desorption of cadmium and tetracycline on cinnamon soil, Chemosphere 80 (2010) 807–812.
[53] P. Kulshrestha, R.F.J.R. Giese, D.S. Aga, Investigating the molecular interactions of oxytetracycline in clay and organic matter: insights on factors affecting its mobility in soil, Environ. Sci. Technol. 38 (2004) 4097–4105.
[54] H. Dolliver, S. Gupta, S. Noll, Antibiotic degradation during manure composting, J. Environ. Qual. 37 (2008) 1245–1253.
[55] O.A. Arikan, W. Mulbry, C. Rice, Management of antibiotic residues from agricultural sources: use of composting to reduce chlortetracycline residues in beef manure from treated animals, J. Hazard. Mater. 164 (2009) 483–489.
[56] I. Chopra, Tetracycline analogs whose primary target is not the bacterial ribosome, Antimicrob. Agents Chemother. 38 (1994) 637–640.